arXiv:2106.05597v1 [cs.CV] 10 Jun 2021

Supervising the Transfer of Reasoning Patterns in VQA

Corentin Kervadec[1]*
Orange Innovation
Cesson-Sévigné, France
corentinkervadec.github.io

Christian Wolf*
LIRIS, INSA Lyon
UMR CNRS 5205, France
christian.wolf@insa-lyon.fr

Grigory Antipov
Orange Innovation
Cesson-Sévigné, France
grigory.antipov@orange.com

Moez Baccouche
Orange Innovation
Cesson-Sévigné, France
moez.baccouche@orange.com

Madiha Nadri
LAGEPP, Univeristé de Lyon
Univ. Claude Bernard, France
madiha.nadri@lagep.univ-lyon1.fr

Abstract

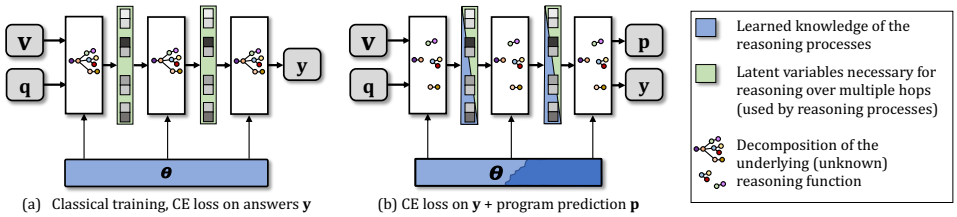
Methods for Visual Question Anwering (VQA) are notorious for leveraging dataset biases rather than performing reasoning, hindering generalization. It has been recently shown that better reasoning patterns emerge in attention layers of a state-of-the-art VQA model when they are trained on perfect (oracle) visual inputs. This provides evidence that deep neural networks can learn to reason when training conditions are favorable enough. However, transferring this learned knowledge to deployable models is a challenge, as much of it is lost during the transfer. We propose a method for knowledge transfer based on a regularization term in our loss function, supervising the sequence of required reasoning operations. We provide a theoretical analysis based on PAC-learning, showing that such program prediction can lead to decreased sample complexity under mild hypotheses. We also demonstrate the effectiveness of this approach experimentally on the GQA dataset and show its complementarity to BERT-like self-supervised pre-training.

1 Introduction

Reasoning over images is the main goal of Visual Question Anwering (VQA), a task where a model is asked to answer questions over images. This problem is a test bed for the creation of agents capable of high-level reasoning, as it involves multi-modal and high-dimensional data as well as complex decision functions requiring latent representations and multiple hops. State-of-the-art models are notorious for leveraging dataset biases and shortcuts in learning rather than performing reasoning, leading to lack of generalization, as evidenced by extensive recent work on bias oriented benchmarks for vision-and-language reasoning [1, 22, 23, 37]. Even large-scale semi-supervised pre-training methods, which successfully managed to increase overall VQA performance, still struggle to address questions whose answers are rare given a context [22].

*Both authors contributed equally. [1] Also at LRIS, INSA Lyon

Preprint. Under review.



(a) Classical training, CE loss on answers **y** (b) CE loss on **y** + program prediction **p**

Figure 1: VQA takes visual input $\boldsymbol{v}$ and a question $\boldsymbol{q}$ and predicts a distribution over answers $\boldsymbol{y}$. (a) Classical discriminative training encodes the full reasoning function in the network parameters θ, while the network activations contain latent variables necessary for reasoning over multiple hops. (b) Additional program supervision requires intermediate network activations to contain information on the reasoning process, simplifying learning the reasoning function g. Under the hypothesis of it's decomposition into multiple reasoning modes, intermediate supervision favors separately learning the mode selector and each individual mode function. This intuition is analyzed theoretically in section 4.

It has been recently shown that reasoning patterns emerge in attention layers of a SOTA VQA model when trained on perfect (oracle) visual inputs, which provides evidence that deep neural networks can learn to reason, when training conditions are favorable enough [23]. In particular, uncertainty and noise in visual inputs seems to be a major cause for shortcut learning in VQA. While this kind of methods provide strong empirical results and insights on the bottlenecks in problems involving learning to reason, they still suffer from significant loss in reasoning capabilities during the transfer phase, when the model is required to adapt from perfectly clean visual input to the noisy input it will encounter after deployment. We conjecture, that reasoning on noisy data involves additional functional components not necessary in the clean case due to different types of domain shifts: (1) a *presence shift*, caused by imperfect object detectors, leading to missing visual objects necessary for reasoning, or to multiple (duplicate) detections; (2) an *appearance shift* causing variations in object embeddings (descriptors) for the same class of objects due to different appearance.

In this paper, we propose a new method for transferring reasoning patterns from models learned on perfect visual input to models trained on noisy visual representations. Key to the success is a regularization term minimizing loss of the reasoning capabilities during transfer. In particular, we address this problem through program prediction as an additional auxiliary loss, i.e. supervision of the sequence of reasoning operations along with their textual and/or visual arguments. To maintain a strong link between the learned function and its objective during the knowledge transfer phase, when inputs are switched from clean oracle inputs to noisy input, the neural model is required to continue to predict complex reasoning programs from different types of inputs.

As a second justification, we claim that program supervision in itself leads to a simpler learning problem, as the underlying reasoning function is decomposed into a set of tasks, each of which is easier to learn individually than the full joint decision function. We backup this claim through a theoretical analysis showing decreased sample complexity under mild hypotheses.

In an experimental study, we demonstrate the effectiveness of this approach on the GQA dataset and show its complementarity when combined to BERT-like self-supervised pre-training [36, 11].

As a summary, we present the following contributions: **(i)** we propose a new program supervision module added on top of vision-language transformer models; **(ii)** we provide a theoretical analysis of the benefit of supervising program prediction in VQA deriving bounds on sample complexity; **(iii)** we experimentally demonstrate the efficiency of program supervision and show that it increases VQA performance on both in- and out-of-distribution sets, even when combined with BERT-like pre-training [36, 11], and that it improves the quality of oracle transfer initially proposed by [23].

2 Related Work

Transformers in VQA — VQA as a task was introduced in various datasets [4, 13, 18], including GQA [17] which is automatically-generated from real-world images. This growing amount of diverse datasets has been accompanied by the development of more and more sophisticated VQA models. While their exhaustive survey is out of the scope of this paper, one can mention some foundational categories of approaches, e.g. those based on object-level attention [2] and tensor decomposition [6]. In this work, we focus on VQA models which are based on Transformers [40], due to their wide

adoption and their impressive results in several tasks (including VQA). In particular, we rely on the combination of Transformers with a large-scale BERT [11]-like pretraining which was shown to be beneficial for VQA in recent works [21, 36]. More recently, [23] focused on the study of so-called reasoning patterns in such Transformer-based VQA models. The authors analyzed how various VQA tasks are encoded in different attention heads, by applying an energy-based analysis inspired by [30]. The analysis was performed using a perfect-sighted oracle Transformer model (which is trained with near-to-perfect visual information, and thus, is much less prone to exploit dataset biases) in order to identify which patterns lead to better reasoning. Then, the authors showed that these reasoning patterns can be transferred from the oracle to a Transformer-based VQA model, thus improving both overall accuracy and accuracy on infrequent answers. In this work, we argue that using program prediction as an additional supervision signal is a catalyst for the transfer of these reasoning patterns.

Biases and shortcut learning in VQA — In addition to the popular VQA datasets mentioned above, other benchmarks were proposed to evaluate specific reasoning capabilities of VQA systems. In particular, they address the issue of shortcut learning [12] in deep learning, where models learn decision rules which are ineffective when tested on a domain or distribution different from the training one. For instance, VQA-CP [1] explicitly inverts the answer distribution between train and test splits. To cope with recent criticisms regarding these evaluations [38, 34], the GQA-OOD dataset [20] introduced a new split of GQA focusing on rare (Out-Of-Distribution / OOD) question-answer pairs, and showed that many VQA models strongly rely on dataset biases. Following this work, the VQA-CE dataset [9] introduced a new evaluation approach related to the VQA v2 dataset. By studying the multi-modal shortcuts in the training set and mining some trivial predictive rules (e.g. co-occurrences of words and visual objects), the evaluation set is generated using questions where these mined rules lead to incorrect answers. As for GQA-OOD, this dataset demonstrated that SOTA models do not perform well when they can't rely on shortcuts, even models which use bias-reduction techniques. Based on these benchmarks, several methods have been conceived to reduce shortcut learning in VQA (see [38, 35] for a comprehensive study of the different techniques). However none of them achieve significant performance improvement on GQA-OOD [20] or VQA-CE [9].

Connections with symbolic VQA — Our work is also related to neuro-symbolic reasoning [42, 29] and neural module networks (NMN) [3, 15], which generally encode a set of pre-defined functions into unique neural modules, then dynamically compose them to execute question-related programs. Several improvements of standard NMNs have been proposed to make them end-to-end trainable through reinforcement learning [19] or, more recently, to enhance their scalability and generalizability [7]. However, the common point of all these works is that they are generally based on the prediction of reasoning programs whose elementary functions are learned jointly with program prediction itself, through program supervision. In contrast to this work, our approach uses program supervision to enrich its internal representations instead of inferring program's execution.

Measuring complexity of learning problems — and thus generalization, has been a goal of theoretical machine learning since the early days, with a large body of work based on PAC-Learning [39, 33]. Traditionally, bounds have been provided ignoring data distributions and focusing uniquely on hypothesis classes (network structures in neural network language), e.g. as measured by VC-dimension. Surprising experimental results on training networks on random samples have seemingly contradicted learning theory [44], in particular Rademacher Complexity. Recently, building on statistics of gradient descent, bounds have been proposed which take into account data distributions, notably [32]. Algorithmic alignment between neural network structures and the decomposition of underlying reasoning functions has been studied in [41], with a focus on algorithms based on dynamic programming. Our theoretical contribution in section 4 builds on the latter two methodologies and extends this type of analysis to intermediate supervision of reasoning programs.

3 Knowledge transfer and program supervision

We propose a method for transferring reasoning patterns from models learned on perfect visual inputs to models trained on noisy visual representations. In the lines of *oracle transfer* [23], we first pre-train a model on ground-truth visual data and then fine-tune on standard visual embeddings extracted with an object detector. The underlying hypothesis is that the noise and uncertainty in visual input prevents the model from learning to reason and leads to learning shortcuts.

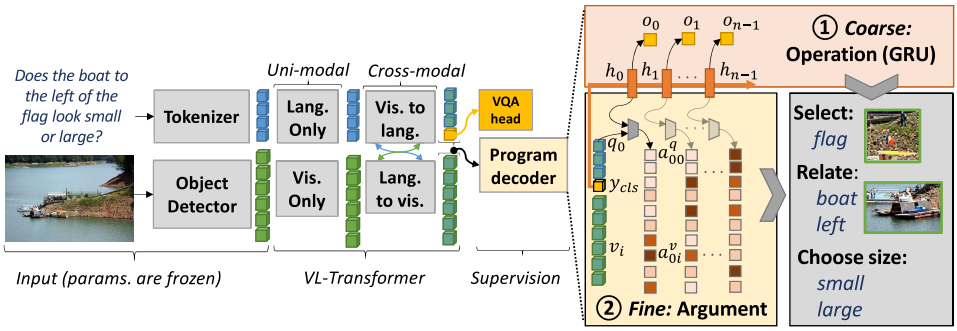


Figure 2: A vision+language transformer with an attached program decoder. The decoder is fed with the VL-Transformer's penultimate embedding (just before the VQA classification head) and generates programs using a coarse-to-fine approach: ① a coarse program is generated using a GRU, consisting of a sequence of program operations embeddings $\{\boldsymbol{o}_i\}_{i\in[0,n-1]}$. ② It is then re-fined by predicting the visual $\boldsymbol{a}^v_{ij}$ and textual $\boldsymbol{a}^q_{ij}$ arguments using an affinity score between operation and input embeddings. Not shown: prediction of the operation's dependencies.

To minimize the loss of reasoning capabilities during the transfer over the *presence shift* between oracle and noisy visual objects, we propose a regularization technique, which supervises the prediction of reasoning steps required to answer the question. We therefore assume the existence of the following ground truth annotation of reasoning programs. A given data sample consists of a sequence $\{\boldsymbol{q}_i\}$ of input question word embeddings, a set $\{\boldsymbol{v}_i\}$ of input visual objects, the ground truth answer class $\boldsymbol{y}^*$ as well as the groundtruth reasoning program, which is structured as a tree involving operations and arguments. Operations $\{\boldsymbol{o}^*_i\}$ are elements of a predefined set {`choose color`, `filter size`, ...}. The arguments of these operations may be taken from (i) all question words, (ii) all visual objects, (iii) all operations — when an operation takes as argument the result of another operation. Hence, arguments are annotated as many-to-many relationships. In the question "*Is there a motorbike or a plane?*", for instance, the operation "or" depends on the result of the two operations checking the existence of a specific object in the image. This is denoted as $\boldsymbol{a}^{q*}_{ij}\in\{0,1\}$ where $\boldsymbol{a}^{q*}_{ij}=1$ means that operation i is associated with question word j as argument and, similarly, $\boldsymbol{a}^{v*}_{ij}=1$ indicating a visual argument and $\boldsymbol{a}^{d*}_{ij}=1$ an operation result argument.

We propose to apply the regularization on top of the VL-Transformer architecture proposed in [36], based on sequences of self- and cross-modality attention. For this purpose, we define a trainable module for program generation (*program decoder*), added to the output of the VL-Transformer model as shown in Fig. 2 — an adaptation to other architectures would be straightforward.

Program decoder — In the lines of [7], the program decoder has been designed in a coarse-to-fine fashion. It first generates ① a coarse sketch of the program consisting only of the operations, which are then ② refined by predicting textual and visual arguments and dependencies between operations.

① **Coarse: operation** — this module only predicts the sequence of operations $\{\boldsymbol{o}_i\}_{i\in[0,n-1]}$ using a recurrent neural network (RNN / GRU) [8] variant, whose initial hidden state is initialized with the y_{CLS} token embedding of the VQA transformer — the same embedding from which classically the final answer $\boldsymbol{y}$ is predicted, *cf.* Figure 2. Inference is stopped when the special "*STOP*" operation is predicted. At each GRU time step i, a new hidden state $\boldsymbol{h}_i$ is computed, from which the operation $\boldsymbol{o}_i$ is classified with a linear projection. It is supervised with a cross-entropy loss $\mathcal{L}_{op}=\sum_i\mathcal{L}_{CE}(\boldsymbol{o}_i,\boldsymbol{o}^*_i)$.

② **Fine: input arguments** — the coarse program is then refined by predicting the operations' arguments. We first deal with textual and visual arguments only. Affinity scores $\boldsymbol{a}^q_{ij}$ between each operation's hidden embedding $\boldsymbol{h}_i$ and each token embedding $\boldsymbol{q}_j$ are computed with a 2-layer feed-forward network from concatenated embeddings. They represent the probability of the word $\boldsymbol{q}_j$ to belong to the argument set of operation $\boldsymbol{o}_i$. Similar scores $\boldsymbol{a}^v_{ij}$ are computed for operations and visual objects. They are supervised with BCE losses $\mathcal{L}_{qarg}=\sum_{ij}\mathcal{L}_{BCE}(\boldsymbol{a}^q_{ij},\boldsymbol{a}^{q*}_{ij})$ and $\mathcal{L}_{varg}=\sum_{ij}\mathcal{L}_{BCE}(\boldsymbol{a}^v_{ij},\boldsymbol{a}^{v*}_{ij})$.

Fine: op arguments — next the dependencies are predicted, i.e. arguments which correspond to results of other operations, and which structure the program into a tree. We deal with these arguments differently, and compute the set of dependency arguments for each operation o_i with another GRU,

whose hidden state is initialized with the hidden state $\boldsymbol{h}_i$ of the operation. The argument index a_{ij}^d is a linear projection of the hidden state and supervised with BCE: $\mathcal{L}_{varg} = \sum_{ij} \mathcal{L}_{BCE}(\boldsymbol{a}_{ij}^d, \boldsymbol{a}_{ij}^{d*})$.

Program supervision — The coarse-to-fine program decoder is trained with the four additional losses weighted by hyperparameters α, β, γ, δ.

$$\mathcal{L} = \underbrace{\mathcal{L}_{vqa}}_{\text{VQA}} + \underbrace{\alpha.\mathcal{L}_{op} + \beta.\mathcal{L}_{dep} + \gamma.\mathcal{L}_{qarg} + \delta.\mathcal{L}_{varg}}_{\text{Program supervision}}, \tag{1}$$

Ground truth programs — We use ground truth information from the GQA [17] dataset, whose questions have been automatically generated from real images. Each sample contains a program describing the operations and arguments required to derive the answer for each question. However, the GT programs have been created for GT visual arguments (GT objects), which do not exactly match the visual input of an object detector used during training and inference [2]. We therefore construct a soft target, by computing intersection-over-union (IoU) between GT and detected objects.

Oracle transfer — Our method uses program supervision to regularize knowledge transfer from a visual oracle to noisy input, as introduced in [23]. Oracle transfer consists in pretraining the VL-Transformer model on ground-truth one-hot visual inputs before performing BERT-like pre-training. It offers training conditions which are more favorable for learning reasoning capabilities. We perform the following steps: **(1)** Oracle pre-training on GT visual input on the GQA dataset; **(2)** (optionally) BERT-like pre-training on data from GQA *unbalanced*; **(3)** Finetuning on the final VQA-objective on the GQA dataset. Each one of these steps are regularized using program supervision.

4 Sample complexity of program supervision

We provide a theoretical analysis indicating that the prediction and supervision of reasoning programs can improve learnability in vision and language reasoning under some assumptions. In what follows, we denote with g "true" (but unknown) underlying reasoning functions, and by f functions approximating them, implemented as neural networks. The goal is to learn a function g able to predict a distribution $\boldsymbol{y}$ over answer classes given an input question and an input image, see Fig 1a. While in the experimental part we use state-of-the-art tranformer based models, in this theoretical analysis, we consider a simplified model, which takes as input the two vectorial embeddings $\boldsymbol{q}$ and $\boldsymbol{v}$ corresponding to, respectively, the question and the visual information (image), for instance generated by a language model and a convolutional neural network, and produces answers $\boldsymbol{y}^* = g(\boldsymbol{q}, \boldsymbol{v})$.

We restrict this analysis to two-layer MLPs, as they are easier to handle theoretically than modern attention based models. The reasoning function g is approximated by neural network f parametrized by a vector θ and which predicts output answers $\boldsymbol{y} = f(\boldsymbol{q}, \boldsymbol{v}, \theta)$.

Our analysis uses PAC-learning [39] and builds on recent results providing bounds on sample complexity taking into account the data distribution itself. We here briefly reproduce Theorem 3.5. from paper [41], which, as an extension of a result in [32], provides a bound for sample complexity of overparametrized MLPs with vectorial outputs, i.e. MLPs with sufficient capacity for learning a given task:

Theorem 4.1 (Sample complexity for overparametrized MLPs)**.** *Let $\mathcal{A}$ be an overparametrized and randomly initialized two-layer MLP trained with gradient descent for a sufficient number of iterations. Suppose $g : \mathbb{R}^d \to \mathbb{R}^m$ with components $g(x)^{(i)} = \sum_j \alpha_j^{(i)} (\beta_j^{(i)T} x)^{p_j^{(i)}}$, where $\beta_j^{(i)} \in \mathbb{R}^d$, $\alpha^{(i)} \in \mathbb{R}$, and $p_j^{(i)} = 1$ or $p_j^{(i)} = 2l, l \in \mathbb{N}_+$. The sample complexity $\mathcal{C}_A(g, \epsilon, \delta)$ is*

$$\mathcal{C}_A(g, \epsilon, \delta) = O\left(\frac{\max_i \sum_j p_j^{(i)} |\alpha_j^{(i)}| \cdot ||\beta_j^{(i)}||_2^{p_j^{(i)}} + \log(\frac{m}{\delta})}{(\epsilon/m)^2} \right) \tag{2}$$

We use the following *Ansatz*: since each possible input question requires a potentially different form of reasoning over the visual content, our analysis is based on the following assumption.

Assumption 1. *The unknown reasoning function $g()$ is a mixture model which decomposes as follows*

$$\boldsymbol{y}^* = \sum_r \boldsymbol{\pi}_r \boldsymbol{h}_r = \sum_r \boldsymbol{\pi}_r g_r(\boldsymbol{v}), \tag{3}$$

where the different mixture components r correspond to different forms of reasoning related to different questions. The mixture components can reason on the visual input only, and the mixture weights are determined by the question $\boldsymbol{q}$, i.e. the weights $\boldsymbol{\pi}$ depend on the question $\boldsymbol{q}$, e.g. $\boldsymbol{\pi} = g_\pi(\boldsymbol{q})$.

We call $g_\pi(.)$ the *reasoning mode estimator*. One hypothesis underlying this analysis is that learning to predict reasoning programs allows the model to more easily decompose into this form (3), i.e. that the network structure closely mimicks this decomposition, as information on the different reasoning modes r is likely to be available in the activations of intermediate layers, *cf.* Figure 1. This will be formalized in assumption 3 and justified further below.

Considering the supposed "true" reasoning function $\boldsymbol{y}^* = g(\boldsymbol{q}, \boldsymbol{v})$ and its decomposition given in (3), we suppose that each individual reasoning module g_r can be approximated with a multi-variate polynomial, in particular each component $\boldsymbol{h}_r^{(i)}$ of the vector $\boldsymbol{h}_r$, as

$$\boldsymbol{h}_r^{(i)} = g_r(\boldsymbol{v}) = \sum_j \alpha_{r,j}^{(i)} (\beta_{r,j}^{(i)T} \boldsymbol{v})^{p_{r,j}^{(i)}} \quad \text{with parameters} \quad \omega = \left\{ \alpha_{r,j}^{(i)}, \beta_{r,j}^{(i)}, p_{r,j}^{(i)}. \right\} \tag{4}$$

A trivial lower bound on the complexity of the reasoning mode estimator $g_\pi(.)$ is the complexity of the identity function, which is obtained in the highly unlikely case where the question embeddings $\boldsymbol{q}$ contain the 1-in-K encoding of the choice of reasoning mode r. We adopt a more realistic case as the following assumption.

Assumption 2. *The input question embeddings $\boldsymbol{q}$ are separated into clusters according to reasoning modes r, such that the underlying reasoning mode estimator g_π can be realized as a NN classifier with dot-product similarity in this embedding space.*

Under this assumption, the reasoning mode estimator can be expressed as a generalized linear model, i.e. a linear function followed by a soft-max σ,

$$\boldsymbol{\pi} = g_\pi(\boldsymbol{q}) = \sigma\left(\left[\gamma_0^T \boldsymbol{q},\ \gamma_1^T \boldsymbol{q}, ...\right]\right), \tag{5}$$

where the different γ_r are the cluster centers of the different reasoning modes r in the question embedding space. As the softmax is a monotonic non-linear function, its removal will not decrease sample complexity[2], and the complexity can be bounded by the logits $\boldsymbol{\pi}_r = \gamma_r^T \boldsymbol{q}$. Plugging this into (3) we obtain that each component $\boldsymbol{y}^{*(i)}$ of the answer is expressed as the following function:

$$\boldsymbol{y}^{*(i)} = \sum_r \left(\gamma_r^T \boldsymbol{q}\right) \sum_j \alpha_{r,j}^{(i)} (\beta_{r,j}^{(i)T} \boldsymbol{v})^{p_{r,j}^{(i)}} \tag{6}$$

We can reparametrize this function by concatenating the question $\boldsymbol{q}$ and the visual input $\boldsymbol{v}$ into a single input vector $\boldsymbol{x}$, which are then masked by two different binary masks, which can be subsumed into the parameters γ_r and $\beta_{r,j}^{(i)}$, respectively, giving

$$\boldsymbol{y}^{*(i)} = \sum_r \sum_j (\gamma_r^T \boldsymbol{x}) \alpha_{r,j}^{(i)} (\beta_{r,j}^{(i)T} \boldsymbol{x})^{p_{r,j}^{(i)}} \tag{7}$$

Extending Theorem 3.5. from [41], we can give our main theoretical result as the sample complexity of this function expressed as the following theorem.

Theorem 4.2 (Sample complexity for multi-mode reasoning functions)**.** *Let $\mathcal{A}$ be an over-parametrized and randomly initialized two-layer MLP trained with gradient descent for a sufficient number of iterations. Suppose $g : \mathbb{R}^d \to \mathbb{R}^m$ with components $g(x)^{(i)} = \sum_r \sum_j (\gamma_r^T \boldsymbol{x}) \alpha_{r,j}^{(i)} (\beta_{r,j}^{(i)T} \boldsymbol{x})^{p_{r,j}^{(i)}}$ where $\gamma_r \in \mathbb{R}^d$, $\beta_{r,j}^{(i)} \in \mathbb{R}^d$, $\alpha_{r,j}^{(i)} \in \mathbb{R}$, and $p_{r,j}^{(i)} = 1$ or $p_{r,j}^{(i)} = 2l, l \in \mathbb{N}_+$. The sample complexity $\mathcal{C}_A(g, \epsilon, \delta)$ is*

$$\mathcal{C}_A(g, \epsilon, \delta) = O\left(\frac{\max_i \sum_r \sum_j \pi p_{r,j}^{(i)} |\alpha| \cdot ||\gamma_r||_2 \cdot ||\beta_{r,j}||_2^{p_{r,j}^{(i)}} + \log(m/\delta)}{(\epsilon/m)^2} \right).$$

[2] In principle, there should exist special degenerate cases, where an additional softmax could reduce sample complexity; however, in our case it is applied to a linear function and thus generates a non-linear function.

The proof of this theorem is given in the supplementary material (Appendix A).

Theorem 4.2 provides the sample complexity of the reasoning function $g()$ under classical training. In the case of program supervision, our analysis is based on the following assumption (see also Fig. 1b):

Assumption 3. *Supervising reasoning programs encodes the choice of reasoning modes r into the hidden activations of the network f. Therefore, learning is separated into several different processes,*

- *(a) learning of the reasoning mode estimator $g_\pi()$ approximated as a network branch $f_\pi()$ connected to the program output;*
- *(b) learning of the the different reasoning modules $g_r()$ approximated as network branches $f_r()$ connected to the different answer classes $\boldsymbol{y}_r$; each one of these modules is learned independently.*

We justify Assumption 3.a through supervision directly, which separates $g_\pi()$ from the rest of the reasoning process. We justify Assumption 3.b by the fact, that different reasoning modes r will lead to different hidden activations of the network. Later layers will therefore see different inputs for different modes r, and selector neurons can identify responsible inputs for each branch $f_r()$, effectively switching off irrelevant input.

We can see that these complexities are lower than the sample complexity of the full reasoning function given in theorem 4.2, since for a given combination of i, r, j, the term $||\gamma_r||_2 \cdot ||\beta_{r,j}||_2^{p_{r,j}^{(i)}}$ dominates the corresponding term $||\beta_{r,j}||_2^{p_{r,j}^{(i)}}$. Let us recall that the different vectors γ correspond to the cluster centers of reasoning modes in language embedding space. Under the assumption that the language embeddings $\boldsymbol{q}$ have been created with batch normalization, a standard technique in neural vision and language models, each value $\gamma_r^{(i)}$ follows a normal distribution $\mathcal{N}(0,1)$. Dropping indices i, r, j to ease notation, we can then compare the expectation of the term $||\gamma||_2 \cdot ||\beta||_2^p$ over the distribution of γ and derive the following relationship:

$$\mathbb{E}_{\gamma^{(i)} \sim N(0,1)} ||\gamma||_2 \cdot ||\beta||_2^p \;=\; C||\beta||_2^p \;=\; \sqrt{2}\frac{\Gamma(\frac{m}{2}+\frac{1}{2})}{\Gamma(\frac{m}{2})}||\beta||_2^p \tag{8}$$

where Γ is the Gamma special function and m is the dimension of the language embedding γ. We provide a proof for this equality in the supplementary material (Appendix A).

Discussion and validity of our claims — the difference in sample complexity is determined by the factor C in equation (8), which monotonically grows with the size of the embedding space m, which is typically in the hundreds. For the order of m=512 to m=768 used for state-of-the-art LXMERT models [36], complexity grows by a factor of around $\sim$20.

We would like to point out, that this analysis very probably under-estimates the difference in complexity, as the difference very much depends on the complexity of the reasoning estimator $\boldsymbol{\pi}$, which we have simplified as a linear function in equation (5). Taking into account just the necessary soft-max alone would probably better appreciate the difference in complexity between the two methods, which we leave for future work. Our analysis is also based on several assumptions, among which is the simplified model (an over-parametrized MLP instead of an attention based network), as well as assumptions of Theorem 4.2 from [41] and [32], on which our analysis is based.

Lastly, we would like to comment on the fact that we compare two different bounds: (i) the bound on sample complexity for learning the full multi-modal reasoning given in Theorem 4.2, and (ii) the bound for learning a single reasoning mode given by Theorem 4.1. While comparing bounds does not provide definitive answers on the order of models, both bounds have been derived by the same algebraic manipulations and we claim that they are comparable.

5 Experimental results

Setup + architecture: — we perform our experiments with a compact version of the Vision-Language (VL)-Tansformer used in [36] (cf. Fig. 2), with a hidden embedding size of d=128 and h=4 heads per layer (only 26M trainable parameters). **Dataset:** our models are trained on the

	Model	Oracle transf.	Prog. sup.	GQA-OOD [20] acc-tail	GQA-OOD [20] acc-head	GQA [17] test-dev	GQA [17] binary*	GQA [17] open*	GQA [17] test-std	AUC† prog.
scratch	(a) Baseline			42.9	49.5	52.4	-	-	-	/
	(b) Oracle transfer	✓		48.2±0.3	54.6±1.1	57.0±0.3	74.5	42.1	57.3	/
	(c) Ours	✓	✓	**48.8**±0.1	**56.1**±0.3	**57.8**±0.2	**75.4**	**43.0**	**58.2**	97.1
+ lxmert	(d) Baseline			47.5	55.2	58.5	-	-	-	/
	(e) Oracle transfer	✓		47.1	54.8	58.4	77.1	42.6	58.8	/
	(f) **Ours**	✓	✓	**48.0**±0.6	**56.6**±0.6	**59.3**±0.3	**77.3**	**44.1**	**59.7**	96.4

Table 1: Impact of program supervision on *Oracle transfer* [23] for vision-language transformers. LXMERT [36] pre-training is done on the GQA unbalanced training set. We report scores on GQA [17] (*test-dev* and *test-std*) and GQA-OOD (*test*). * binary and open scores are computed on the test-std; † we evaluate visual argument prediction by computing AUC@0.66 on GQA-val.

Ablations	GQA-OOD [20] acc-tail (val.)	GQA [17] val.
(1) VQA only	46.9	62.2
(2) Coarse only	46.5	62.5
(3) Coarse + dep.	46.8	62.8
(4) Full w/o v.arg	47.3	63.7
(5) Full (ours)	**49.9**	**66.2**

Table 2: Ablation of different types of program supervision (compact model, no LXMERT/BERT pre-training, no Oracle), on GQA val. *v.arg* = superv. of visual arguments.

Ablations	GQA-OOD [20] acc-tail (val.)	GQA [17] val.
(6) No prog	50.0	66.4
(7) Uni-modal	49.9	66.5
(8) Cross-modal	**50.4**	**67.4**

Table 3: We study the impact of the program supervision posistion: after uni-modal layers or after cross-modal layers (*standard configuration*). The supervision is more efficient when used after cross-modal interactions. Setting=oracle transfer, no lxmert

balanced GQA [17] training set (∼1M question-answer pairs). However, LXMERT pretraining is done on the *unbalanced* training set (∼15M question-answer pairs). The latter contains more questions and programs, but the same number of images (∼100K images). **Evaluation:** is performed on GQA [17] and GQA-OOD [20] test sets. GQA is a dataset with question-answer pairs automatically generated from real images, and is particularly well suited for evaluating a large variety of reasoning skills. GQA-OOD is a benchmark dedicated to the out-of-domain VQA evaluation, and gives information on the generalization capabilities of the model. Hyper-parameters are selected either on the testdev (for GQA) or validation (for GQA-OOD) sets. When specified (with ±) we provide the average accuracy and standard deviation computed on three runs with different random seeds. **Visual input:** following [2], we use bottom-up visual features extracted using a pre-trained object detector (we keep its parameters frozen during the training). If not specified, we use faster-RCNN [31] with 36 objects per-images. In addition to that, we experiment with designed objects, and also with the VinVL [45] features which (unlike faster-RCNN ones) are conceived specifically for vision-language tasks.

Program supervision improves visual reasoning — Tab. 1 reports the effectiveness of program prediction when combined with oracle and BERT-like pretraining on the GQA dataset and corroborates the results found in the theoretical analysis. In addition, when using both program supervision and LXMERT [36] but without oracle transfer, we achieve an accuracy of 58.8 on the *testdev* set of GQA. This is lower than oracle transfer's accuracy, demonstrating the complementary of the two methods. We note that the majority of the gain is achieved on the more challenging *open* questions. In addition, results on GQA-OOD (*acc-tail* and *acc-head*) suggest that the gains are obtained in, both, out- and in-distribution settings. However, as already observed in [23], LXMERT pre-training tends to decrease the *acc-tail* gains brought by oracle transfer plus program supervision. We evaluate the program prediction performance by measuring the area under the ROC curve (AUC) on the visual argument prediction with an IoU treshold of $\frac{2}{3}$=0.66. Models (c) and (e) achieve, respectively, 97.1 and 96.4 AUC scores, demonstrating the effectiveness of the program decoder.

Visual arguments are the key — We study the impact of different types of program supervision in Tab. 2. We can see the importance of supervising arguments, in (4) and (5). The supervision of visual arguments (5) contributes most to the gain in performance, again corroborating that visual uncertainty is the main bottleneck for reasoning on the GQA dataset.

Program supervision enhances cross-modal interactions — In Tab. 3, we study how the inputs of the program prediction module influence the VQA accuracy. In particular, we test two settings: (7)

Model	Visual features	Oracle transf.	Prog. sup.	GQA [17] test-dev	binary*	open*	test-std
(g) Oracle transfer	100 RCNN [2]	✓		57.0$_{\pm 0.4}$	-	-	-
(h) Ours		✓	✓	**58.2**$_{\pm 0.1}$	-	-	-
(i) Oracle transfer	VinVL [45]	✓		59.6$_{\pm 0.1}$	-	-	-
(j) Ours		✓	✓	60.9$_{\pm 0.2}$	-	-	-
(k) Oracle transfer +lxmert		✓		61.4	79.6	47.5	62.5
(l) Ours +lxmert		✓	✓	**61.8**	**80.1**	**48.0**	**63.0**

Table 4: Impact of improved visual inputs while using program supervision on Vision-Language Transformers. Scores on GQA [17]. *binary/open are computed on test-std.

Method	Visual feats.	Additional supervision	Training data (M) Img	Sent	GQA-OOD [20] acc-tail	acc-head	GQA [17] bin.	open	all
BAN4 [24]	RCNN [2]	-	≈ 0.1	≈ 1	47.2	51.9	76.0	40.4	57.1
MCAN [43]	RCNN [2]	-	≈ 0.1	≈ 1	46.5	53.4	75.9	42.2	58.0
Oracle transfer [23]	RCNN [2]	-	≈ 0.18	≈ 1	48.3	55.5	75.2	44.1	58.7
MMN [7]	RCNN [2]	Program	≈ 0.1	≈ 15	48.0	55.5	78.9	44.9	60.8
LXMERT [36]	RCNN [2]	-	≈ 0.18	≈ 9	**49.8**	57.7	77.8	45.0	60.3
Ours	VinVL [45]	Program	≈ 0.1	≈ 15	49.1	**59.7**	80.1	48.0	63.0
NSM [16]	SG [16]	Scene graph	≈ 0.1	≈ 1	-	-	78.9	**49.3**	63.2
OSCAR$_{+\text{VinVL}}$ [45]	VinVL [45]	-	≈ 5.7	≈ 9	-	-	**82.3**	48.8	**64.7**

Table 5: Comparison with the state of the art on the GQA [17] (*test-std*) and GQA-OOD [20] (*test*) sets. For a fair comparison, we provide information about the required training data and supervision.

uni-modal, where the programs are predicted from the vision and language embeddings right after the uni-modal layers (language and vision only in Fig. 2); and (8) *cross-modal*, where the programs are predicted after the cross-modal layers (as shown in Fig. 2). We observe that, contrary to the latter, the former does not improve the baseline ((7) vs (6) in Tab. 3). This highlights the fact that the program supervision mainly impacts the operations in the cross modal layers, where the most complex reasoning operations are performed.

Program supervision allows to take advantage of the improved visual inputs — We analyse the impact of using our method with a better input image representation. Increasing the number of objects from 36 to 100 per image ((g) and (h) in Tab. 4), allows to further increase the gains brought by our method. On the contrary, the score of the baseline model remains unchanged, showing that the program supervision allows to take advantage of a bigger number of object proposals. Similarly, replacing the faster-RCNN features by the more recent and more accurate VinVL ones ((i)-(l) in Tab. 4) results in better performances.

Comparison with SOTA — We report in Tab. 5 the results obtained by our approach compared to the current SOTA on the GQA and GQA-OOD datasets. In order to ensure a fair comparison, we also provide, for each method, information regarding the amount of data (images and sentences) used during training. As shown in Tab. 5, our approach compares favourably with SOTA since it obtains the second best accuracy (with a 0.2 points gap) on the GQA test-std set among the approaches which not use extra training data. The results also remain competitive when comparing to the OSCAR$_{+\text{VinVL}}$ [45], while being trained with 50 times less images. On GQA-OOD, our approach obtains the second best *acc-tail* score (and the best *acc-head* one) with a much less complex architecture than current SOTA (26M vs 212M trainable parameters compared to LXMERT [36]).

6 Conclusion

We have demonstrated that it is possible to improve the reasoning abilities of VQA models when providing additional supervision of program annotations. In particular, our method is designed to improve the transfer of reasoning patterns from models learned on perfect visual input to models trained on noisy visual representations. Our experiments are supported by a theoretical analysis, demonstrating that program supervision can decrease sample complexity under reasonable hypothesis. The proposed method relies on the availability of reasoning program annotations, which are costly to annotate, especially when dealing with human generated questions. Recent work has already

managed to gather such kind of annotations [10]. The next step will be to extend the method to configurations where the program annotation is rare or incomplete.

Broader Impact — Beyond the exciting scientific reasons for exploring work on visual reasoning, we welcome the potentially high interest for society in VQA systems targeting increased accessibility. As an example, we have tools in mind, which allow the visually impaired to query their environment based on visual information from a wearable camera. We are currently not aware of existing applications abusing VQA systems for unethical goals. Potential future unethical abuse, generally and beyond our contribution, could involve their use to automatic solving of Captchas (automatic Turing tests), and the creation of false dialogs and discussions in online forums ("troll farms") requiring the examination of posted text as well as accompanying images. The latter is a risk inherent to any powerful system capable of predicting text, but for the moment does not realistically apply to VQA, where very short answers are predicted through classification over the full answer dictionary (even though our contribution is independent of the chosen VQA model).

References

[1] Aishwarya Agrawal, Dhruv Batra, Devi Parikh, and Aniruddha Kembhavi. Don't just assume; look and answer: Overcoming priors for visual question answering. In *CVPR*, 2018.

[2] Peter Anderson, Xiaodong He, Chris Buehler, Damien Teney, Mark Johnson, Stephen Gould, and Lei Zhang. Bottom-up and top-down attention for image captioning and visual question answering. In *CVPR*, pages 6077–6086, 2018.

[3] Jacob Andreas, Marcus Rohrbach, Trevor Darrell, and Dan Klein. Neural module networks. In *CVPR*, 2016.

[4] Stanislaw Antol, Aishwarya Agrawal, Jiasen Lu, Margaret Mitchell, Dhruv Batra, C Lawrence Zitnick, and Devi Parikh. Vqa: Visual question answering. In *ICCV*, 2015.

[5] Jimmy Lei Ba, Jamie Ryan Kiros, and Geoffrey E Hinton. Layer normalization. *arXiv preprint arXiv:1607.06450*, 2016.

[6] Hedi Ben-Younes, Rémi Cadene, Matthieu Cord, and Nicolas Thome. Mutan: Multimodal tucker fusion for visual question answering. In *ICCV*, 2017.

[7] Wenhu Chen, Zhe Gan, Linjie Li, Yu Cheng, William Wang, and Jingjing Liu. Meta module network for compositional visual reasoning. In *WACV*, 2021.

[8] Kyunghyun Cho, Bart van Merrienboer, Çaglar Gülçehre, Dzmitry Bahdanau, Fethi Bougares, Holger Schwenk, and Yoshua Bengio. Learning phrase representations using rnn encoder-decoder for statistical machine translation. In *EMNLP*, 2014.

[9] Corentin Dancette, Remi Cadene, Damien Teney, and Matthieu Cord. Beyond question-based biases: Assessing multimodal shortcut learning in visual question answering. *arXiv preprint arXiv:2104.03149*, 2021.

[10] Abhishek Das, Harsh Agrawal, C. Lawrence Zitnick, Devi Parikh, and Dhruv Batra. Human Attention in Visual Question Answering: Do Humans and Deep Networks Look at the Same Regions? In *EMNLP*, 2016.

[11] Jacob Devlin, Ming-Wei Chang, Kenton Lee, and Kristina Toutanova. Bert: Pre-training of deep bidirectional transformers for language understanding. In *Conference of the North American Chapter of the Association for Computational Linguistics: Human Language Technologies*, 2019.

[12] Robert Geirhos, Jörn-Henrik Jacobsen, Claudio Michaelis, Richard Zemel, Wieland Brendel, Matthias Bethge, and Felix A Wichmann. Shortcut learning in deep neural networks. *Nature Machine Intelligence*, 2(11):665–673, 2020.

[13] Yash Goyal, Tejas Khot, Douglas Summers-Stay, Dhruv Batra, and Devi Parikh. Making the v in vqa matter: Elevating the role of image understanding in visual question answering. In *CVPR*, pages 6904–6913, 2017.

[14] Dan Hendrycks and Kevin Gimpel. Gaussian error linear units (gelus). *arXiv preprint arXiv:1606.08415*, 2016.

[15] Ronghang Hu, Jacob Andreas, Marcus Rohrbach, Trevor Darrell, and Kate Saenko. Learning to reason: End-to-end module networks for visual question answering. In *Proceedings of the IEEE International Conference on Computer Vision*, pages 804–813, 2017.

[16] Drew Hudson and Christopher D Manning. Learning by abstraction: The neural state machine. In *Advances in Neural Information Processing Systems*, pages 5901–5914, 2019.

[17] Drew A Hudson and Christopher D Manning. Gqa: A new dataset for real-world visual reasoning and compositional question answering. In *CVPR*, pages 6700–6709, 2019.

[18] Justin Johnson, Bharath Hariharan, Laurens van der Maaten, Li Fei-Fei, C Lawrence Zitnick, and Ross Girshick. Clevr: A diagnostic dataset for compositional language and elementary visual reasoning. In *CVPR*, pages 2901–2910, 2017.

[19] Justin Johnson, Bharath Hariharan, Laurens Van Der Maaten, Judy Hoffman, Li Fei-Fei, C Lawrence Zitnick, and Ross Girshick. Inferring and executing programs for visual reasoning. In *Proceedings of the IEEE International Conference on Computer Vision*, pages 2989–2998, 2017.

[20] C. Kervadec, G. Antipov, M. Baccouche, and C. Wolf. Roses Are Red, Violets Are Blue... but Should VQA Expect Them To? *Pre-print: arxiv:2006.05121*, 2020.

[21] Corentin Kervadec, Grigory Antipov, Moez Baccouche, and Christian Wolf. Weak supervision helps emergence of word-object alignment and improves vision-language tasks. In *European Conference on Artificial Intelligence*, 2019.

[22] Corentin Kervadec, Grigory Antipov, Moez Baccouche, and Christian Wolf. Roses are red, violets are blue... but should vqa expect them to? In *CVPR*, 2021.

[23] Corentin Kervadec, Theo Jaunet, Grigory Antipov, Moez Baccouche, Romain Vuillemot, and Christian Wolf. How transferable are reasoning patterns in vqa? In *CVPR*, 2021.

[24] Jin-Hwa Kim, Jaehyun Jun, and Byoung-Tak Zhang. Bilinear attention networks. In *Advances in Neural Information Processing Systems*, pages 1564–1574, 2018.

[25] Diederik P Kingma and Jimmy Ba. Adam: A method for stochastic optimization. 2014.

[26] Ranjay Krishna, Yuke Zhu, Oliver Groth, Justin Johnson, Kenji Hata, Joshua Kravitz, Stephanie Chen, Yannis Kalantidis, Li-Jia Li, David A Shamma, et al. Visual genome: Connecting language and vision using crowdsourced dense image annotations. *IJCV*, 123(1):32–73, 2017.

[27] Alexandre Lacoste, Alexandra Luccioni, Victor Schmidt, and Thomas Dandres. Quantifying the carbon emissions of machine learning. *arXiv preprint arXiv:1910.09700*, 2019.

[28] Tsung-Yi Lin, Michael Maire, Serge Belongie, James Hays, Pietro Perona, Deva Ramanan, Piotr Dollár, and C Lawrence Zitnick. Microsoft coco: Common objects in context. In *ECCV*, 2014.

[29] Jiayuan Mao, Chuang Gan, Pushmeet Kohli, Joshua B. Tenenbaum, and Jiajun Wu. The Neuro-Symbolic Concept Learner: Interpreting Scenes, Words, and Sentences From Natural Supervision. In *International Conference on Learning Representations*, 2019.

[30] Hubert Ramsauer, Bernhard Schäfl, Johannes Lehner, Philipp Seidl, Michael Widrich, Lukas Gruber, Markus Holzleitner, Milena Pavlović, Geir Kjetil Sandve, Victor Greiff, et al. Hopfield networks is all you need. *arXiv preprint arXiv:2008.02217*, 2020.

[31] Shaoqing Ren, Kaiming He, Ross Girshick, and Jian Sun. Faster r-cnn: Towards real-time object detection with region proposal networks. In *Advances in neural information processing systems*, pages 91–99, 2015.

[32] S.S. Du S. Arora, W. Hu, Z. Li, and R. Wang. Fine-grained Analysis of optimization and generalization for overparametrized two-layer neural networks. In *ICML*, 2019.

[33] Shai S. Shalev-Shwart and S. Ben-David. *Understanding Machine Learning - From Theory to Algorithms*. Cambridge University Press, 2014.

[34] Robik Shrestha, Kushal Kafle, and Christopher Kanan. A negative case analysis of visual grounding methods for vqa. In *Proceedings of the 58th Annual Meeting of the Association for Computational Linguistics*, 2020.

[35] Robik Shrestha, Kushal Kafle, and Christopher Kanan. An investigation of critical issues in bias mitigation techniques. *arXiv preprint arXiv:2104.00170*, 2021.

[36] Hao Tan and Mohit Bansal. Lxmert: Learning cross-modality encoder representations from transformers. In *EMNLP*, pages 5103–5114, 2019.

[37] Damien Teney, Ehsan Abbasnejad, and Anton van den Hengel. Unshuffling data for improved generalization. *arXiv preprint arXiv:2002.11894*, 2020.

[38] Damien Teney, Ehsan Abbasnejad, Kushal Kafle, Robik Shrestha, Christopher Kanan, and Anton van den Hengel. On the value of out-of-distribution testing: An example of goodhart's law. In *NeurIPS*, 2020.

[39] L.G. Valiant. A theory of the learnable. In *Communications of the ACM*, volume 27(11), 1984.

[40] Ashish Vaswani, Noam Shazeer, Niki Parmar, Jakob Uszkoreit, Llion Jones, Aidan N Gomez, Łukasz Kaiser, and Illia Polosukhin. Attention is all you need. In *Advances in neural information processing systems*, pages 5998–6008, 2017.

[41] K. Xu, J. Li, M. Zhang, S.S. Du, K.-I. K., and S. Jegelka. What can Neural Networks Reason About. In *ICLR*, 2020.

[42] Kexin Yi, Jiajun Wu, Chuang Gan, Antonio Torralba, Pushmeet Kohli, and Joshua B Tenenbaum. Neural-Symbolic VQA: Disentangling Reasoning from Vision and Language Understanding. In *Advances in Neural Information Processing Systems (NIPS)*, 2018.

[43] Zhou Yu, Jun Yu, Yuhao Cui, Dacheng Tao, and Qi Tian. Deep modular co-attention networks for visual question answering. In *CVPR*, pages 6281–6290, 2019.

[44] C. Zhang, S. Bengio, M. Hardt, B. Recht, and O. Vinyals. Understanding deep learning requires rethinking generalization . In *ICLR*, 2017.

[45] Pengchuan Zhang, Xiujun Li, Xiaowei Hu, Jianwei Yang, Lei Zhang, Lijuan Wang, Yejin Choi, and Jianfeng Gao. Vinvl: Making visual representations matter in vision-language models. *arXiv preprint arXiv:2101.00529*.

Supplementary Material

A Proofs of Section 4

A.1 Proof of theorem 4.2

For the unfamiliar reader, we here briefly recall the notion of sample complexity, in the context of PAC-learning [39], which characterizes the minimum amount (=M) of samples necessary to learn a function with sufficiently low ($=\epsilon$) error with sufficiently high ($=\delta$) probability:

Definition A.1 (Sample complexity)**.** Given an error threshold $\epsilon>0$; a threshold on error probability δ; a training set $S=\{x_i, y_i\}$ of M i.i.d. training samples from $\mathcal{D}$, generated from some underlying true function $\boldsymbol{y}_i = g(\boldsymbol{x}_i)$, and a learning algorithm $\mathcal{A}$, which generates a function f from training data, e.g. $f=\mathcal{A}(S)$; Then g is (M,ϵ,δ)-learnable by $\mathcal{A}$ if

$$\mathbb{P}_{x\sim D}\left[||f(x)-g(x)||\leq\epsilon\right]\geq 1-\delta \tag{9}$$

The case of scalar outputs In the lines of [32], we first define the case for a single component $\boldsymbol{y}^{(i)}$ of the vector $\boldsymbol{y}$ and define the following Corollary:

Corollary 0.1 (Sample complexity for multi-mode reasoning functions with a single scalar component)**.** *Let $\mathcal{A}$ be an overparametrized and randomly initialized two-layer MLP trained with gradient descent for a sufficient number of iterations. Suppose $g:\mathbb{R}^d\to\mathbb{R}^m$ with $g(x)=\sum_r\sum_j(\gamma_r^T\boldsymbol{x})\alpha_{r,j}(\beta_{r,j}^T\boldsymbol{x})^{p_{r,j}}$ where $\gamma_r\in\mathbb{R}^d$, $\beta_{r,j}\in\mathbb{R}^d$, $\alpha_{r,j}\in\mathbb{R}$, and $p_{r,j}=1$ or $p_{r,j}=2l, l\in\mathbb{N}_+$. The sample complexity $\mathcal{C}_A(g,\epsilon,\delta)$ is*

$$\mathcal{C}_{\mathcal{A}}(g,\epsilon_0,\delta_0)=O\left(\frac{\sum_r\sum_j\pi p_{r,j}|\alpha|\cdot||\gamma_r||_2\cdot||\beta_{r,j}||_2^{p_{r,j}}+\log(\frac{1}{\delta_0})}{\epsilon_0^2}\right),$$

Proof of Corollary 0.1:

Using Theorem 5.1 from [32], we know that sums of learnable functions are learnable, and can thus focus on a single term

$$y=g(\boldsymbol{x})=\alpha(\gamma^T\boldsymbol{x})(\beta^T\boldsymbol{x})^p \tag{10}$$

where we dropped indices r and j and the superscript (i) for convenience.

We proceed in the lines of the proof of Theorem 5.1 in [32]. Given a set of i.i.d data samples $S=\{(\boldsymbol{x}_s,y_s)\}_{s=1}^n=(\boldsymbol{X},\boldsymbol{y})$ from the underlying function $g(x)$, let $\boldsymbol{w}$ be the weights of the first layer of two layer network with ReLu activations; let $\boldsymbol{H}^\infty\in\mathbb{R}^{n,n}$ be a Gram matrix defined as follows, with elements

$$\boldsymbol{H}_{ij}^\infty=\mathbb{E}_{\boldsymbol{w}\sim\mathcal{N}(0,1)}\left[\boldsymbol{x}_i^T\boldsymbol{x}_j\mathbb{I}\{\boldsymbol{w}^t\boldsymbol{x}_i\geq 0,\boldsymbol{w}^t\boldsymbol{x}_i\geq 0\}\right].$$

To provide bounds on the sample complexity of $g(x)$, using Theorem 5.1 of [32], it suffices to show that the following bound holds

$$\sqrt{\boldsymbol{y}^T(\boldsymbol{H}^\infty)^{-1}\boldsymbol{y}}<M_g \tag{11}$$

for a bound M_g independent of the number of samples n.

For first introduce some notation. For matrices $\boldsymbol{A}=[\boldsymbol{a}_1,...,\boldsymbol{a}_{n_3}]\in\mathbb{R}^{n_1\times n_3}$ and $\boldsymbol{B}=[\boldsymbol{b}_1,...,\boldsymbol{b}_{n_3}]\in\mathbb{R}^{n_2\times n_3}$, the *Khatri-Rao* product is defined as $\boldsymbol{A}\odot\boldsymbol{B}=[\boldsymbol{a}_1\otimes\boldsymbol{b}_1,\boldsymbol{a}_2\otimes\boldsymbol{b}_2,...,\boldsymbol{a}_{n_3}\otimes\boldsymbol{b}_{n_3}]$. Let $\circ$ be the *Haddamard* product (element wise multiplication) of two matrices. We also denote the corresponding powers by $\boldsymbol{A}^{\otimes l},\boldsymbol{A}^{\odot l},\boldsymbol{A}^{\circ l}$. We denote by $\boldsymbol{A}^\dagger=(\boldsymbol{A}^T\boldsymbol{A})^{-1}\boldsymbol{A}^T$ the *Moore-Penrose* pseudo-inverse, and by $\boldsymbol{P}_{\boldsymbol{A}}=\boldsymbol{A}^{\frac{1}{2}}\boldsymbol{A}^\dagger\boldsymbol{A}^{\frac{1}{2}}$ the projection matrix for the subspace spanned by $\boldsymbol{A}$.

From the proof of Theorem 5.1 in [32], we also know that

$$\boldsymbol{H}^\infty\succeq\frac{\boldsymbol{K}^{\circ 2l}}{2\pi(2l-1)^2},$$

where $\boldsymbol{K} = \boldsymbol{X}^T\boldsymbol{X}$, and $\boldsymbol{X}$ is the data matrix of all row vectors $\boldsymbol{x}_i$.

Let us consider the case of $p = 1$. Reformulating equation (10), we get:

$$y = g(\boldsymbol{x}) = \alpha(\gamma^T\boldsymbol{x})(\beta^T\boldsymbol{x}) \tag{12}$$
$$= \alpha(\boldsymbol{x}^T\gamma)(\boldsymbol{x}^T\beta) \tag{13}$$
$$= \alpha(\boldsymbol{x}\otimes\boldsymbol{x})^T(\gamma\otimes\beta) \tag{14}$$

Now, taking the full set of input vectors $\boldsymbol{x}_i$ arranged into the full data matrix $\boldsymbol{X}$, we can perform similar algebraic operations to get

$$\boldsymbol{y} = g(\boldsymbol{X}) = \alpha(\boldsymbol{X}^T\gamma) \circ (\boldsymbol{X}^T\beta) \tag{15}$$
$$= \alpha(\boldsymbol{X}^{\odot 2})^T(\gamma\otimes\beta) \tag{16}$$

Plugging (15) and (16) into (11), we need to show that the following expression is smaller than a constant M_g:

$$\alpha^2((\boldsymbol{X}^T\gamma) \circ (\boldsymbol{X}^T\beta))^T(\boldsymbol{H}^\infty)^{-1}(\boldsymbol{X}^{\odot 2})^T(\gamma\otimes\beta) \tag{17}$$
$$=\alpha^2((\boldsymbol{X}^{\odot 2})^T(\gamma\otimes\beta))^T(\boldsymbol{H}^\infty)^{-1}(\boldsymbol{X}^{\odot 2})^T(\gamma\otimes\beta) \tag{18}$$
$$=\alpha^2(\gamma\otimes\beta)^T(\boldsymbol{X}^{\odot 2})(\boldsymbol{H}^\infty)^{-1}(\boldsymbol{X}^{\odot 2})^T(\gamma\otimes\beta) \tag{19}$$
$$\leq 2\pi\alpha^2(\gamma\otimes\beta)^T(\boldsymbol{X}^{\odot 2})(\boldsymbol{K}^{\circ 2})^\dagger(\boldsymbol{X}^{\odot 2})^T(\gamma\otimes\beta) \tag{20}$$
$$=2\pi\alpha^2(\gamma\otimes\beta)^T\boldsymbol{P}_{\boldsymbol{X}^{\odot 2}(\boldsymbol{X}^{\odot 2})^T}(\gamma\otimes\beta) \tag{21}$$
$$\leq 2\pi\alpha^2||(\gamma\otimes\beta)||_2^2 \tag{22}$$
$$=2\pi\alpha^2||\gamma||_2^2 \cdot ||\beta||_2^2 \tag{23}$$

where we made use of $||a\otimes b||_2^2 = ||a||_2^2||b||_2^2$ for two vectors a and b and an integer n.

This finishes the proof for the case $p = 1$.

Let us consider the case of $p = 2l+1$. Reformulating equation (10), we get:

$$\boldsymbol{y} = g(\boldsymbol{X}) = \alpha(\boldsymbol{X}^T\gamma) \circ (\boldsymbol{X}^T\beta)^p \tag{24}$$
$$= \alpha(\boldsymbol{X}^{\odot 2l})^T(\gamma\otimes\beta^{\otimes(2l+1)}) \tag{25}$$

Plugging (25) into (11), we again need to show that the following expression is smaller than a constant M_g:

$$\alpha^2((\boldsymbol{X}^{\odot 2l})^T(\gamma\otimes\beta^{\otimes(2l+1)}))^T \tag{26}$$
$$(\boldsymbol{H}^\infty)^{-1}(\boldsymbol{X}^{\odot 2l})^T(\gamma\otimes\beta^{\otimes(2l+1)}) \tag{27}$$
$$=\alpha^2(\gamma\otimes\beta^{\otimes(2l+1)})^T \tag{28}$$
$$(\boldsymbol{X}^{\odot 2l})(\boldsymbol{H}^\infty)^{-1}(\boldsymbol{X}^{\odot 2l})^T(\gamma\otimes\beta^{\otimes(2l+1)}) \tag{29}$$
$$\leq 2\pi(2l-1)^2\alpha^2(\gamma\otimes\beta^{\otimes(2l+1)})^T \tag{30}$$
$$(\boldsymbol{X}^{\odot 2l})(\boldsymbol{K}^{\circ 2})^\dagger(\boldsymbol{X}^{\odot 2l})^T(\gamma\otimes\beta^{\otimes(2l+1)}) \tag{31}$$
$$=2\pi(2l-1)^2\alpha^2(\gamma\otimes\beta^{\otimes(2l+1)})^T \tag{32}$$
$$\boldsymbol{P}_{\boldsymbol{X}^{\odot 2l}(\boldsymbol{X}^{\odot 2l})^T}(\gamma\otimes\beta^{\otimes(2l+1)}) \tag{33}$$
$$\leq 2\pi(2l-1)^2\alpha^2||(\gamma\otimes\beta^{\otimes(2l+1)})||_2^2 \tag{34}$$
$$\leq 2\pi p^2\alpha^2||(\gamma\otimes\beta^{\otimes(2l+1)})||_2^2 \tag{35}$$
$$=2\pi p^2\alpha^2||\gamma||_2^2 \cdot ||\beta||_2^{2p} \tag{36}$$

where we made use of $||a\otimes b||_2^2 = ||a||_2^2||b||_2^2$ and therefore $||a^{\otimes n}||_2^2 = ||a||_2^{2n}$ for two vectors a and b and an integer n.

This finishes the proof for the case $p = 2l+1$.

The case of vectorial outputs In the lines of [41], we consider each component of the output vector independent and apply an union bound to Corollary 0.1. If the individual components $\boldsymbol{y}^{(i)}$ fail to learn with probability δ_0, then the full output of dimension m fails with probability $m\delta_0$ and with an error of at most $m\epsilon_0$. A change of variables from (ϵ_0, δ_0) to (ϵ, δ) gives a complexity for the model with vectorial output of

$$\mathcal{C}_A(g, \epsilon, \delta) = O\left(\frac{\max_i \sum_r \sum_j \pi p_{r,j}^{(i)} |\alpha| \cdot ||\gamma||_2 \cdot ||\beta_{r,j}||_2^{p_{r,j}^{(i)}} + \log(m/\delta)}{(\epsilon/m)^2}\right),$$

This ends the proof of Theorem 4.2.

A.2 Proof of the inequality in Eq. (8)

Let us denote by $p(x)$ the density of normal distribution. And to make the notation more succinct and to avoid confusion between different usages of superscripts, in this proof we will change γ_r^i to γ_i, i.e. the ith component of the vector γ, not to be confused with γ_r, a vector corresponding to the embedding of the rth reasoning mode. Then,

$$\mathbb{E}_{\gamma_i \sim N(0,1)} ||\gamma||_2 \cdot ||\beta||_2^p \tag{37}$$

$$= ||\beta||_2^p \mathbb{E}_{\gamma_i \sim N(0,1)} \left(\sum_i \gamma_i^2\right)^{\frac{1}{2}} \tag{38}$$

$$\tag{39}$$

We now perform a change of variables and introduce a new random variable

$$z = \sum_i \gamma_i^2. \tag{40}$$

Since each individual γ_i is distributed normal, z is distributed according to a χ^2 distribution with m degrees of freedom, and we get

$$\mathbb{E}_{\gamma_i \sim N(0,1)} ||\gamma||_2 \cdot ||\beta||_2^p \tag{41}$$

$$= ||\beta||_2^p \, \mathbb{E}_{z \sim \chi^2}[z^{\frac{1}{2}}] \tag{42}$$

The expectation now corresponds to $\frac{1}{2}^{th}$ centered moment of the χ^2 distribution with m degrees of freedom, whose kth moments are given as

$$\mathbb{E}_{z \sim \chi^2}[z^k] = 2^k \frac{\Gamma(\frac{m}{2} + k)}{\Gamma(\frac{m}{2})} \tag{43}$$

This ends the proof of the equality.

B Program decoder

We provide more details on the program decoder architecture. The hidden size is set to 128 (same as in the VL-Transformer). We use GeLU [14] as non linearity, along with layernorm [5].

Operations The maximum number of operations in one program is set to $N_{maxop} = 9$. The total number of operation's labels is $N_{op} = 212$. We use a one layer GRU [8] with hidden size equals to 128, to infer the operation's hidden embedding $\boldsymbol{h}_i$. It is followed by a two layers MLP ($128 \to 64 \to N_{op}$, projecting $\boldsymbol{h}_i$ into a one-hot vector $\boldsymbol{o}_i$.

Arguments Affinity scores $\boldsymbol{a}_{ij}^q$ between each operation's hidden embedding $\boldsymbol{h}_i$ and each token embedding $\boldsymbol{q}_j$ (or $\boldsymbol{v}_j$) are computed with a 2-layer feed-forward network ($256 \to 64 \to 1$) from concatenated embeddings. The op arguments are predicted from $\boldsymbol{h}_i$ using another one layer GRU with hidden size equals to 128 followed by a nonlinear projection ($128 \to N_{maxop}$).

Table 6: Training and execution time for one run. *Ours* corresponds to oracle transfer plus program prediction. We also provide the approximated amount of runs done during this work (hyper parameters search, abblation, *etc*.)

Run	Model	#GPUs	# hours	Total number of runs
train	Oracle	1	30	≈ 5
train+test	ours 36 RCNN	1	9	≈ 100
train+test	ours 100 RCNN	2	10	≈ 5
train+test	ours VinVL	2	10	≈ 5
train+test	ours 36 RCNN + LXMERT pretrain	2	100	≈ 20
train+test	ours 36 RCNN + LXMERT finetune	1	4	≈ 50
train+test	ours VinVL + LXMERT pretrain	3	180	2
train+test	ours VinVL + LXMERT finetune	1	6	2

Hyper-parameters are set to $\alpha = 1$, $\beta = 1$, $\gamma = 1$ and $\delta = 100$.

C Training details

Architecture: Our VQA architecture is a compact version of the VL-Transformer introduced in [36][3]. In particular, it has 9 language only layers, 5 vision only layers, and 5 cross modal layers. The hidden size is set to 128. In total, this compact version has 26M parameters, allowing to reduce computation time and memory overhead.

Optimizer: All models were trained with the Adam optimizer [25], a learning rate of 10^{-4} with warm starting and learning rate decay.

Oracle transfer: is performed following [23]. First, the oracle model is trained during at most 40 epochs on the GQA *balanced* training set with ground-truth image representation. Then we continue the training during 10 epochs, with visual features extracted using an object detector. We use a batch size equals to 196 (96 when using VinVL features).

BERT/LXMERT [36] pretraining is performed during 20 epochs with a batch size of 320 (256 when using VinVL features). All pretraining losses are added from the beginning, including the VQA one. Note that LXMERT [36] is originally pre-trained on a corpus gathering images and sentences from MSCOCO [28] and VisualGenome [26]. In this work, we only train on the GQA [17] *unbalanced* set, with VisualGenome images. After pre-trainning, we finetune on the GQA [17] *balanced* set during 4 epochs, with a batch size of 32 and a learning rate equal to 10^{-5}.

D Computing resources

Training and evaluation has been performed on several compute infrastructures, which include an Nvidia DGX-A100 with 8$\times$ A100 GPUs and a cluster with P100 and RTX 2080 GPUs. After design and development, the final training and evaluation runs have been performed on Geforce RTX 2080 GPUs. We provide an estimate for the amount of compute in Table 6 — the number of GPUs and approximate execution times for different models and experimental settings (train, validation and test).

C02 Emission The RTX infrastructure has a carbon efficiency of 0.035 kgCO_2eq/kWh. A cumulative of 6500 hours of computation was performed on hardware of type RTX 2080 (TDP of 215W). Total emissions are estimated to be 48.9 kgCO_2eq . Estimations were conducted using the `https://mlco2.github.io/impact#compute` presented in [27].

[3]We use the code publicly available at `https://github.com/airsplay/lxmert`

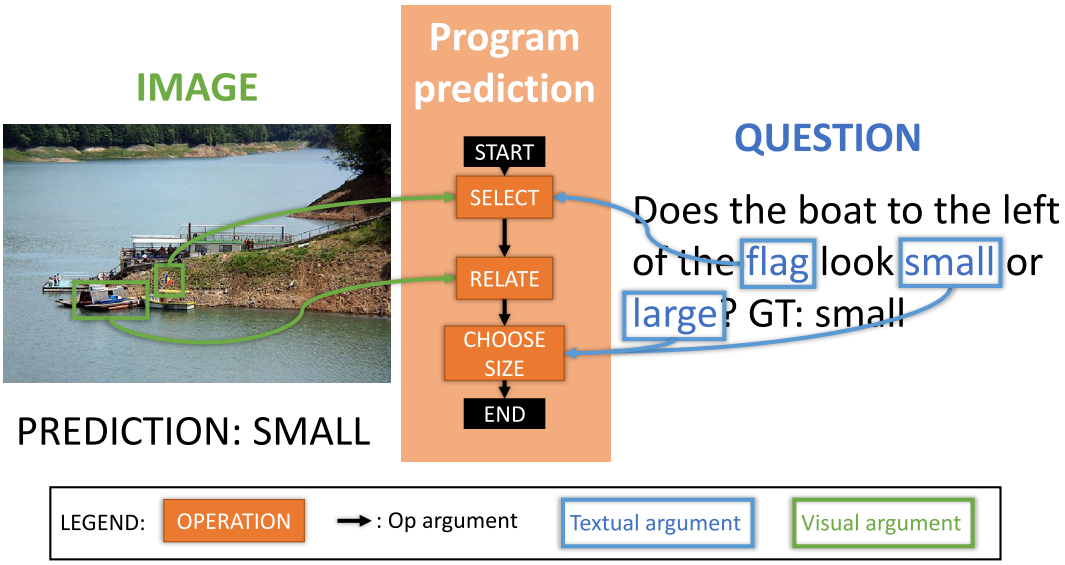


Figure 3: Example of program prediction. The question is: "Does the boat to the left of the flag looks small or large?". Our model (ours+lxmert with VinVL) correctly answers "small".

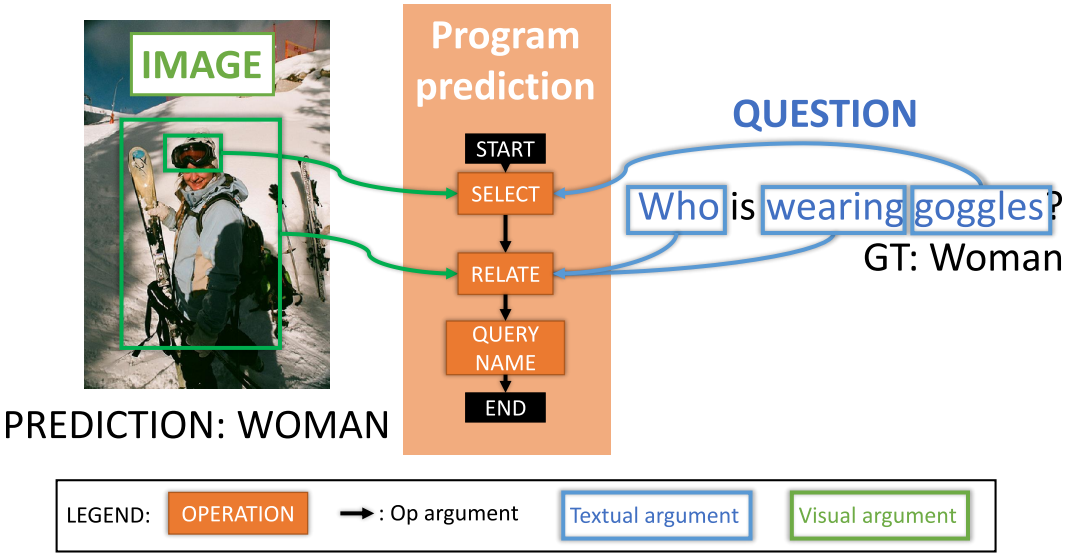


Figure 4: Example of program prediction. The question is: "Who is wearing goggles?". Our model (ours+lxmert with VinVL) correctly answers "woman".

E Visualisation of predictions

We provide example of program prediction in Fig. 3 and 4. In Fig. 3, the question is *'does the boat to the left of the flag look small or large?'*. The program decoder successfully infers the correct program. It first predicts the coarse operations – `select, relate, choose size` –, then adds the arguments taken from the image or the question – boat, flag, small, large –. Finally, the VQA model predicts the correct answer *'small'*. In Fig. 4, the question is *'who is wearing goggles?'*. Similarly to the first example, the program decoder generates coarse operations – `select, relate, query name` – and visual/textual arguments – woman, who, goggles, wearing–. In these two examples, the decoder correctly predicts that the programs are chains of operations (special case of a tree). At contrary, a question like *'are there nuts or vegetables?'* is a not a chain because of the presence of `exist` and `or` operations.

Ablations	GQA-OOD [20] acc-tail (val.)	GQA [17] val.
(1) VQA only	46.9	62.2
(2) Random prog.	45.7	61.4
(3) ours	**49.9**	**66.2**

Table 7: Comparison with the *random prog* baseline, where we randomly replace the ground truth program with a program picked from another question (compact model, no LXMERT/BERT pre-training, no Oracle), on GQA val.

F Sanity check

As a sanity check, and to avoid the unfortunate result pinpointed in [34], we compare our model with a random baseline *random prog.* in Tab. 7. In *random prog.*, we randomly replace the ground truth program with a program picked from another question, during the training. As expected, this random baseline achieves low performances.